Fuel 411 (2026) 137992

Contents lists available at ScienceDirect

Fuel

journal homepage: www.elsevier.com/locate/jfue

Full length article

Operating sensitivities for steam versus co-electrolysis on a commercial solid-oxide electrolysis stack with Power-to-X implications

Felix Mütter[a,*], Pavle Boškoski[b,c], Stefan Megel[d], Christoph Hochenauer[a], Vanja Subotić[a]

[a] Institute of Thermal Engineering, Graz University of Technology, Inffeldgasse 25/B, Graz, 8010, Austria
[b] Jožef Stefan Institute, Department of Systems and Control, Jamova cesta 39, Ljubljana, SI-1000, Slovenia
[c] Faculty of Information Studies, Ljubljanska cesta 31a, Novo mesto, 8000, Slovenia
[d] Fraunhofer Institute of Ceramic Technologies and Systems, Winterbergstrasse 28, Dresden, 01277, Germany

HIGHLIGHTS

- DoE-based quantification of parameter effects on stack voltage (steam EC).
- EIS, DRT, and in-plane temperature diagnostics on a 5-cell commercial stack.
- Same-hardware benchmark: co-electrolysis shows larger per-unit sensitivities.
- At matched production, co-electrolysis requires 2 % higher DC power and kWh Nm^{-3}.

GRAPHICAL ABSTRACT

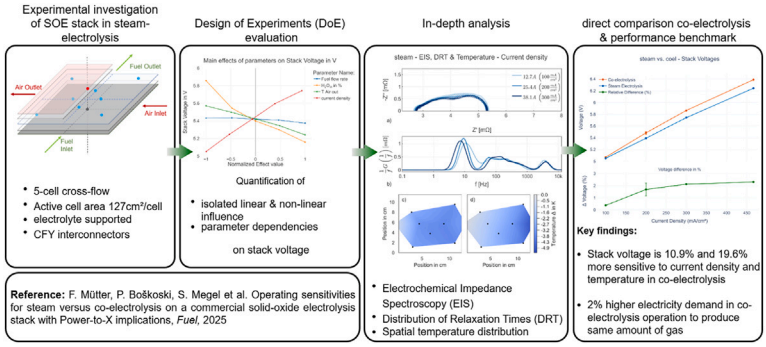

ARTICLE INFO

Keywords:
Design of Experiments (DoE)
Solid Oxide Electrolysis (SOE)
Steam Electrolysis
Hydrogen Production
Co-electrolysis
Power-to-X (PtX)

ABSTRACT

Same-hardware, stack-scale evidence for PtX syngas routes is scarce. We quantify, on identical solid-oxide hardware, how operating conditions affect stack voltage and specific electricity demand to guide selection between steam electrolysis, paired downstream with RWGS, and direct co-electrolysis. We report new stack-level steam-electrolysis data and benchmark them against our previously published co-electrolysis dataset on the same five-cell electrolyte-supported stack and test rig. Measurements are non-overlapping with aligned operating windows and a single analysis pipeline. A structured design-of-experiments with regression yields sensitivities to current density, fuel-side composition/flow, and temperature. Electrochemical impedance spectroscopy (EIS), distribution of relaxation times (DRT), and in-plane temperature mapping provide mechanistic context for ohmic, charge-transfer, and transport contributions. Within the tested window, co-electrolysis shows stronger voltage sensitivity to current density and the air-outlet setpoint. Differences in specific electricity demand are modest per stack yet material at plant scale. Holding hardware and analysis constant, we deliver a reproducible benchmark that supports route selection and informs thermal and current-density control in commercial PtX plants.

1. Introduction

The European Union's ambition of reaching climate neutrality by 2050 has increased the demand for new energy technologies that can both cut fossil fuel use and allow a much larger share of renewables in the overall energy mix [1]. Among the various electrolysis concepts, solid oxide electrolysis (SOE) has gained particular attention.

* Corresponding author.
Email address: felix.muetter@tugraz.at (F. Mütter).

https://doi.org/10.1016/j.fuel.2025.137992
Received 23 September 2025; Received in revised form 2 December 2025; Accepted 9 December 2025
Available online 17 December 2025

One reason is its very high system efficiency, with studies reporting values above 83 % (LHV) [2–4]. Another important aspect is flexibility: SOE can be operated with steam or with a mixture of steam and carbon dioxide, producing hydrogen or syngas depending on the feed. This versatility makes the technology attractive for different Power-to-X routes, helping to decarbonise industries such as aviation or steel production, where greenhouse–gas reductions are challenging. Recent reviews, for example the perspective by Zheng et al. in *Electrochemical Energy Reviews* [3], summarise the development status, remaining materials and system challenges, and Power-to-X integration options for steam and co-electrolysis.

To realise this potential in practice, it is important to understand how changes in operating parameters influence performance and efficiency.

Several studies have looked at steam and co-electrolysis, but often with different aims and experimental scales. Wolf et al. [5] investigated single cells and reported that co-electrolysis appeared to degrade more slowly than the corresponding steam operation. In contrast, Preininger et al. examined both single cells and stacks in reversible operation and pointed out that the reverse water–gas shift (RWGS) reaction is already active at open-circuit voltage, influencing both steam and CO_2 electrolysis from the very beginning [6,7]. The authors in [8] focused on a two-cell anode-supported stack, operated for several hundred hours at two temperatures; their EIS/DRT analysis showed degradation was more pronounced at 700 °C than at 800 °C.

Although valuable, these and other studies mainly addressed degradation behaviour and were often limited to single cells or small short stacks that differ from commercial hardware. At stack and module relevant scale, Königshofer et al. characterised an electrolyte-supported stack that serves as a representative unit of a 150 kW reversible SOC module under system relevant gas mixtures and operating conditions in order to define safe operating strategies for the large-scale module [9]. Even with these contributions, most available work and review articles focus on materials development, degradation mechanisms and system concepts rather than on systematic, stack scale operating sensitivities. What has largely been missing is a systematic, statistically rigorous quantification of how operating parameters affect stack voltage in commercial scale stacks, and a same hardware benchmark under matched DoE ranges and boundary control strategy between steam electrolysis and co-electrolysis.

In our earlier work [10], we quantified parameter effects for co-electrolysis using a Design of Experiments (DoE) approach on a commercial electrolyte-supported (ESC) stack. This approach made it possible to separate and quantify main, quadratic and interaction effects in a statistically consistent way and to highlight which factors most strongly determined stack performance.

The present study builds on this methodology and extends it to steam electrolysis using the same five-cell ESC stack and an identical DoE framework, so that results can be compared directly. We report a new, non-overlapping steam-mode dataset acquired on the identical stack and under the same DoE conditions, enabling a same-hardware benchmark under matched DoE ranges and boundary-control strategy at commercial scale. In addition to quantifying the impact of current density, air-outlet temperature, fuel flow rate and inlet steam fraction, we include complementary electrochemical diagnostics. Electrochemical impedance spectroscopy (EIS), distribution of relaxation times (DRT) and spatial temperature measurements are used to link the observed statistical effects to underlying physical processes such as mass transport, polarisation losses and thermal gradients. This combined approach provides a robust basis for direct comparison of operation modes and supports plant-level decision-making for Power-to-X route selection.

The main contributions of this study are threefold:

- *Quantification of parameter effects*: A statistical evaluation of main, quadratic and interaction effects of four operating parameters on stack voltage during steam electrolysis in a commercial-scale ESC stack.
- *Electrochemical diagnostics*: Additional analysis with EIS, DRT and spatially resolved temperature measurements provides a mechanistic interpretation of the observed parameter sensitivities.
- *Benchmarking of operation modes*: A direct, same-hardware comparison under matched DoE ranges and boundary-control strategy with our previous co-electrolysis study highlights differences in parameter influence and shows the higher power demand of co-electrolysis within the explored operating window.

Together, these results support the optimisation of SOE operation and inform system-level decisions on hydrogen versus syngas production routes.

1.1. Thermodynamics

From a thermodynamic perspective, both steam electrolysis and co-electrolysis are strongly endothermic processes. In the following, the reaction equations for both steam and co-electrolysis are shown, whereby the reaction enthalpies at 800 °C were either taken from the literature [11] or calculated using the software HSC Chemistry 10 from © Metso [12].

The half reactions at the fuel side for steam and CO_2 electrolysis can be written as follows:

$$H_2O + 2e^- \rightleftharpoons H_2 + O^{2-}, \quad \Delta H^\circ_{800} = +1179\ \mathrm{kJ\,mol^{-1}}, \tag{1}$$

$$CO_2 + 2e^- \rightleftharpoons CO + O^{2-}, \quad \Delta H^\circ_{800} = +1213\ \mathrm{kJ\,mol^{-1}}, \tag{2}$$

and the corresponding half reaction at the air electrode is

$$O^{2-} \rightleftharpoons \tfrac{1}{2}O_2 + 2e^-, \quad \Delta H^\circ_{800} = -931\ \mathrm{kJ\,mol^{-1}}. \tag{3}$$

Combining these half reactions yields the overall reactions:

$$H_2O \rightleftharpoons H_2 + \tfrac{1}{2}O_2, \quad \Delta H^\circ_{800} = +248\ \mathrm{kJ\,mol^{-1}}, \tag{4}$$

$$CO_2 \rightleftharpoons CO + \tfrac{1}{2}O_2, \quad \Delta H^\circ_{800} = +282\ \mathrm{kJ\,mol^{-1}}. \tag{5}$$

In a conventional route, CO_2 is converted by combining steam electrolysis with a downstream reverse water–gas shift (RWGS) reactor,

$$CO_2 + H_2 \rightleftharpoons CO + H_2O, \quad \Delta H^\circ_{800} = +34\ \mathrm{kJ\,mol^{-1}}, \tag{6}$$

In co-electrolysis, the electrochemical and RWGS contributions occur simultaneously in the fuel electrode. In thermodynamic terms, the total enthalpy change involved in producing a given syngas composition is comparable for 'steam electrolysis + RWGS' and direct co-electrolysis. However, the distribution of thermal and electrical energy input differs between the stack and any downstream auxiliary reactor.

The interaction between these coupled equilibria and the electrochemical driving force influences the achievable voltage, conversion and product gas composition. Understanding these relationships is therefore essential in order to explain potential differences in the performance of steam electrolysis and co-electrolysis, which provides a motivation for the present comparative study.

2. Experimental setup

2.1. Cell and stack design

All experiments were performed on the same five-cell electrolyte-supported (ESC) stack that was also used in our earlier co-electrolysis study [10]. In the present work, the stack was operated exclusively in steam electrolysis mode in order to allow a direct comparison with the co-electrolysis results.

Each single cell consisted of a screen-printed Ni/GDC fuel electrode with a thickness of approximately 40 μm, a strontium-doped lanthanum manganite (LSM) air electrode about 50 μm thick, and a dense 10Sc1CeSZ electrolyte layer with a thickness of around 165 μm.

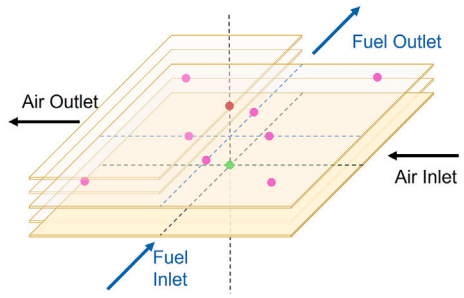

Fig. 1. Schematics of stack flow configuration with thermocouples placed directly in the air flow channel of the middle cell shown as pink ● solid circles. The thermocouples placed outside of the stack on top and bottom are shown as red ● and green ● solid circles, respectively. (For interpretation of the references to colour in this figure legend, the reader is referred to the web version of this article.)

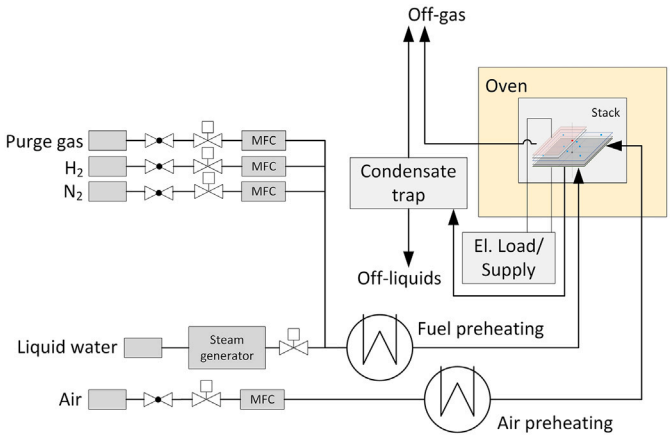

Fig. 2. Schematics of stack test rig for steam electrolysis operation.

The metallic interconnects were produced from powder-processed CFY alloy and had external dimensions of 130 × 150 mm^2. The effective active area of each cell was 127 cm^2, and the stack was operated in a cross-flow configuration.

The open-channel design on the air side made it possible to insert a thermocouple directly into the flow field of the central cell. These in-cell measurements do not provide a fully resolved temperature field and should be regarded as indicative rather than representative of the complete distribution. In addition, type N thermocouples were placed at the fuel and air inlets and outlets, and two type K thermocouples recorded the temperatures at the top and bottom of the stack housing. The overall layout of the flow fields and thermocouple positions is illustrated in Fig. 1. Further background information on this stack type can be found in [6,7,13].

2.2. Test rig

The steam-electrolysis setup used a five-cell electrolyte-supported stack inside a high-temperature furnace. Fuel and air were preheated upstream to near furnace temperature to prevent condensation. Hydrogen and air flow rates were controlled by thermal mass flow controllers (Voegtlin, Switzerland) [14] and steam was supplied by a continuous generator. Downstream, the gases passed through a condenser to remove excess water before safe venting. Although no off-gas analysis was performed, the condenser prevented moisture accumulation in the exhaust and ensured safe handling. The stack was connected to a programmable DC supply for current control and voltage measurement.

Furnace power was adjusted in feedback to hold the stack air-outlet temperature $T_{\mathrm{air,out}}$ at a prescribed setpoint. All experiments were carried out at near-ambient pressure (approximately 1 bar absolute), and stack pressure was not varied as an independent operating parameter. According to the stack manufacturer the maximum allowable pressure difference between the anode and cathode and between each gas channel and the ambient is below 100 mbar, so the stack was operated close to ambient pressure on both sides. A type N thermocouple at the outlet, typically the hottest location, provided the measurement. $T_{\mathrm{air,out}}$ was a design factor in the DoE and was maintained at its level for each run, with the controller compensating for reaction-heat changes with current density to keep $T_{\mathrm{air,out}}$ stable within the tested window. Additional type N thermocouples at the air and fuel inlets and outlets monitored boundary conditions.

A schematic of the rig, including flow paths and sensor positions, is shown in Fig. 2. Relative to our earlier work, the schematic was redrawn and simplified for clarity, and the carbonaceous mass flow controllers were omitted because they were not used in the steam-electrolysis experiments.

2.3. Design of experiments

To systematically evaluate the influence of operating parameters on stack performance, a Design of Experiments (DoE) approach was applied. A central composite inscribed (CCI) test plan was selected, which combines factorial, axial and centre points and is well suited for capturing both linear and nonlinear parameter effects, as well as first-order interactions. In total, 28 experiments were conducted according to this plan, including repeated centre points to assess repeatability and experimental uncertainty.

The four operating parameters investigated were:

- Current density
- Fuel flow rate
- Educt share in the inlet fuel mixture
- Air-outlet temperature of the stack

These parameters were selected because they can be controlled reliably in the test rig and are known to strongly influence both stack voltage and gas conversion. Furthermore, adopting the same parameter set as in our earlier co-electrolysis study [10] ensures direct comparability between the two operation modes, so that observed differences can be attributed to the underlying process rather than to differences in the experimental design. In the present work, the air-outlet temperature denotes the manipulated furnace-control setpoint and not a passive outcome. Its specific role as a control variable and its coupling to current density are discussed in Section 2.2. This choice also reflects typical practice in system-relevant hotbox stack operation, where the air-outlet temperature is used as the reference temperature for stack control to maintain the desired thermal state under varying electrical loads [15]. The variation ranges for all four factors are listed in Table 1, while the air flow rate was kept constant at 30 slpm for all experiments. Conditions were harmonized across modes by using the identical stack and test rig, the same DoE structure and parameter ranges (current density, fuel flow, air-outlet temperature control, air flow), while feed composition necessarily differed between steam electrolysis and co-electrolysis. Throughout this manuscript, educt share means the inlet oxidant fraction at the fuel inlet, equal to $x_{\mathrm{H_2O,in}}$ in steam electrolysis and to $x_{\mathrm{H_2O,in}} + x_{\mathrm{CO_2,in}}$ in co-electrolysis.

The experimental results were evaluated using a quadratic regression model of the form

$$y = \beta_0 + \sum_{i=1}^{4} \beta_i x_i + \sum_{i=1}^{4} \beta_{ii} x_i^2 + \sum_{i=1}^{4} \sum_{j=i+1}^{4} \beta_{ij} x_i x_j,$$

where y denotes the response (e.g. average stack voltage), x_i are the coded values of the four parameters, and β are the regression coefficients. This model structure is standard for CCI designs and enables the quantification of

Table 1
Boundary conditions for the investigated operating parameters.

	Low	Mid	High	Unit
Fuel flow rate	4	5.5	7	slpm
Current density	100	200	300	$\frac{mA}{cm^2}$
Educt share	20	50	80	%
Air-outlet temperature	800	824	847	°C
Air flow rate	30			slpm

- linear effects of each parameter,
- quadratic effects describing curvature, and
- interaction effects capturing the combined influence of two parameters.

In the present study, this regression framework not only provides the statistical basis for identifying parameter sensitivities in steam electrolysis but also serves as a consistent reference for comparison with our earlier co-electrolysis dataset. This comparative application highlights differences in how operating parameters influence the two modes and thereby extends the methodology beyond a single-process analysis. In the present work the primary electrochemical response metric in the design of experiments is the stack voltage, from which the specific electrical energy demand is derived.

2.4. Analysis methods

To allow a direct comparison with our earlier co-electrolysis study [10], the same type of measurement and evaluation procedures were used here. The main steps are summarized in the following.

During the experiments, current, voltage and temperature were monitored continuously. Electrochemical impedance spectroscopy (EIS) was additionally performed at those operating points defined by the test plan, and the spectra were evaluated by means of distribution of relaxation times (DRT) analysis. For the impedance measurements we applied the fast-EIS approach of Boskoski et al. [16], which relies on a pseudo-random binary sequence (PRBS) as an excitation signal. This method covers a wide frequency range within a short acquisition time. The perturbation amplitude was set to 4 % of the applied DC current.

For the DRT evaluation, the recorded spectra were first checked with the Kramers-Kronig (KK) test. Data points with a deviation larger than 3 % from the KK prediction were excluded. The DRT itself was then calculated according to Wan et al. [17], using a Gaussian window, a regularisation factor of 10^{-3} and a shape parameter of 2.25. These values were kept unchanged compared to our previous work to ensure that the results are directly comparable between steam and co-electrolysis.

DRT frequency survey for SOE process interpretation

To help with the interpretation of the DRT spectra, the literature survey that we compiled in [10] was updated and expanded. The overview, shown in Fig. 3, separates fuel- and air-electrode related processes and marks those that are specifically linked to CO_2. It should be read as a working aid rather than a fixed classification, since frequency ranges often overlap and several processes can contribute at the same time.

From the reviewed literature, some general tendencies can nevertheless be pointed out:

- At frequencies below roughly 100 Hz, peaks are usually connected with gas diffusion or conversion processes at both electrodes.
- In the range between about 100 and 1000 Hz, charge transfer and mass transport phenomena dominate, particularly at the air electrode.
- At frequencies above 1000 Hz, features are most often related to ionic transport and charge-transfer processes in the fuel electrode.

The assignments in Fig. 3 should therefore be regarded as indicative trends rather than strict boundaries. They reflect the current state of knowledge in the literature and serve here only as a reference for discussing the experimental spectra.

2.5. Calculation of derived responses

In addition to stack voltage, several derived quantities were calculated in order to place the results in a broader performance context and to ensure comparability with our previous co-electrolysis study [10].

- *Hydrogen production rate:* The hydrogen molar flow rate $\dot{n}_{H_2}$ is defined as follows:

$$\dot{n}_{H_2} = \frac{i\, A_{\text{cell}}\, N_{\text{cell}}}{2\, F \cdot 10^3} \quad \left[\frac{\text{mol}}{\text{s}}\right],$$

with i the applied current density in $\frac{\text{mA}}{\text{cm}^2}$, $A_{\text{cell}} = 127\ \text{cm}^2$ the active electrode area of one cell, $N_{\text{cell}} = 5$ the number of cells in the stack, and $F = 96485\ \frac{\text{C}}{\text{mol}}$ the Faraday constant. The result is obtained in $\frac{\text{mol}}{\text{s}}$.

- *Specific electrical energy demand:* The electrical energy demand per mole of hydrogen e_{mol} is defined as follows:

$$e_{\text{mol}} = 2\, FE,$$

with E the measured stack voltage in V and F the Faraday constant in $\frac{\text{C}}{\text{mol}}$. The result is obtained in $\frac{\text{J}}{\text{mol}}$. For comparison with literature, the value per normal cubic metre e_{Nm^3} is defined as:

$$e_{\text{Nm}^3} = \frac{e_{\text{mol}} \cdot 1000}{3.6 \times 10^6 \cdot 22.414},$$

corresponding to 1 Nm^3 of dry gas at 0 °C and 1 atm (molar volume 22.414 L mol^{-1}). The result is obtained in $\frac{\text{kWh}}{\text{Nm}^3}$.

Electricity price context. Electricity cost assumptions are anchored in Germany's corporate renewable PPA index (IEA, 2023). We use the P50 (median) of the most recent 12-month window (Mar 2022-Mar 2023) as the base case. The P25-P75 band ($e86$-$e103\ \text{MWh}^{-1}$) is used for sensitivity [31].

3. Results and discussion

This section quantifies how the investigated operating parameters in steam electrolysis affect the stack voltage. Effects were estimated using a quadratic response-surface model on coded variables from a central-composite-inscribed design, including all linear terms, first-order interaction terms and quadratic terms. Statistical significance was assessed at $p < 0.05$. For interpretability, we report effect magnitudes in physical units by back-transforming coded coefficients to the experimental ranges. Per-unit effect values and ranked magnitudes are visualized in Fig. 4(b). To link statistics with mechanisms, we discuss the most influential factors using a compact triad consisting of (i) Nyquist/EIS features, (ii) DRT peak behaviour, and (iii) in-plane temperature distributions from the multi-probe measurements.

3.1. Steam electrolysis evaluation - effects on stack voltage

Fig. 4 summarizes the main findings. In panel (a), each factor is varied across its coded range while the others are held at their mid levels; dots show measured voltages. In panel (b), the statistically significant effects (linear, quadratic, first-order interactions) are ranked by magnitude.

Three robust trends emerge:

- Direction of effects. Increasing current density increases voltage (positive effect), whereas increasing air-outlet temperature, inlet steam fraction (educt share, H_2O_{in}), and fuel flow rate decreases voltage (negative effects).
- Curvature. Only H_2O_{in} shows a non-linear trend, which is strong at the low end and weaker at the high end.

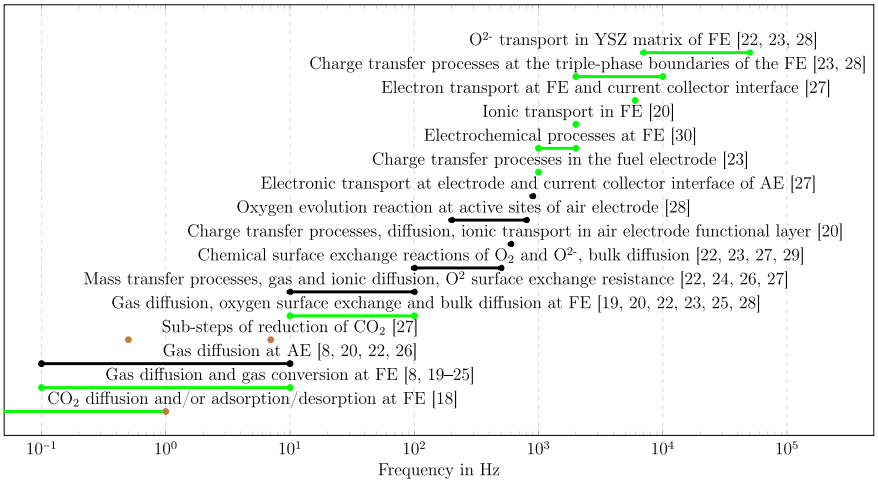

Fig. 3. Overview of processes and mechanisms as a function of DRT frequency from literature. Coloured horizontal lines indicate frequency ranges where processes have commonly been reported: fuel electrode (FE) processes (—), air electrode (AE) processes (—). Brown bullet markers (●) highlight phenomena that are specifically associated with CO_2. The overview is intended as a guide for interpretation rather than a strict classification [18]. (For interpretation of the references to colour in this figure legend, the reader is referred to the web version of this article.)

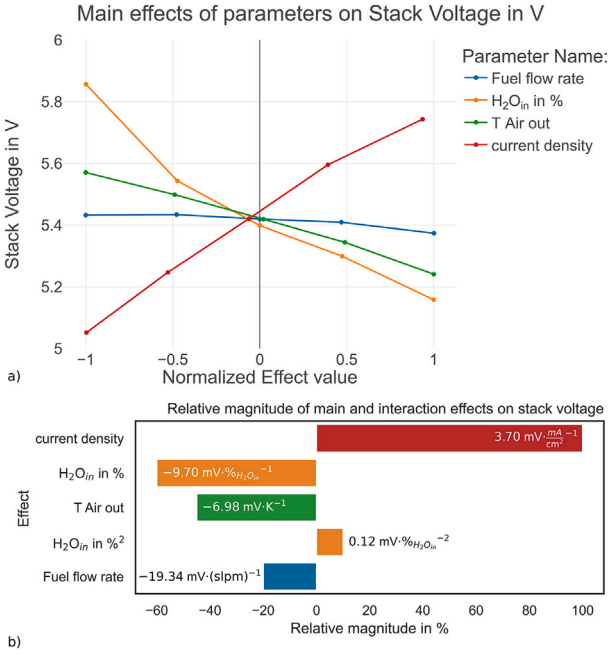

Fig. 4. (a) Main-effect trends for stack voltage in steam electrolysis. Each operating parameter is varied over its coded range $(-1, 0, +1)$ while the others are fixed at their mid levels. Dots represent measured voltages, and connecting lines serve as visual guides (b) Ranked relative magnitudes of statistically significant linear and quadratic main effects and first-order interaction effects from the OLS quadratic model ($p < 0.05$). Bars are normalised to the largest effect and numeric labels indicate the corresponding per-unit sensitivities in physical units (e.g. $mV \cdot \frac{mA}{cm^2}^{-1}$).

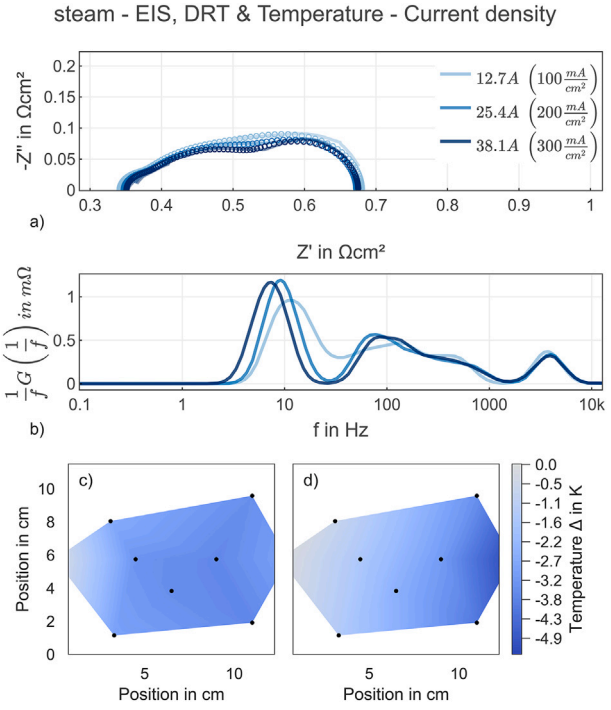

Fig. 5. (a) Nyquist and (b) DRT for current-density changes. The spatial temperature change when increasing the current density from 100 to 200 $\frac{mA}{cm^2}$ and from 200 to 300 $\frac{mA}{cm^2}$ is depicted in (c) and (d), respectively. Fuel enters from the bottom and air flows from right to left in (c) and (d).

- Interactions. No first-order interaction terms reach significance at $p < 0.05$ within the explored ranges.

Per-unit effect magnitudes and the corresponding ranked comparison appear in Fig. 4(b). Effects are given as $\mathrm{mV} \cdot (\mathrm{unit})^{-1}$, where the denominator matches the factor's physical unit ($\mathrm{mA\,cm^{-2}}$, $\%_{H_2O_{in}}$, K, slpm). In the main text we round values to three significant figures.

Current density

In steam electrolysis mode, the current density was the most influential parameter on the stack voltage. An increase in the current density by one $\frac{mA}{cm^2}$ results in an increase in the stack voltage by 3.70 mV.

Despite a slight non-linearity observable in Fig. 4(a) at higher current density values, only a linear influence of the current density was found to be statistically significant. The observed voltage change follows the expected behaviour according to Ohm's law. Fig. 5 provides further details on the influence of the current density on the underlying processes

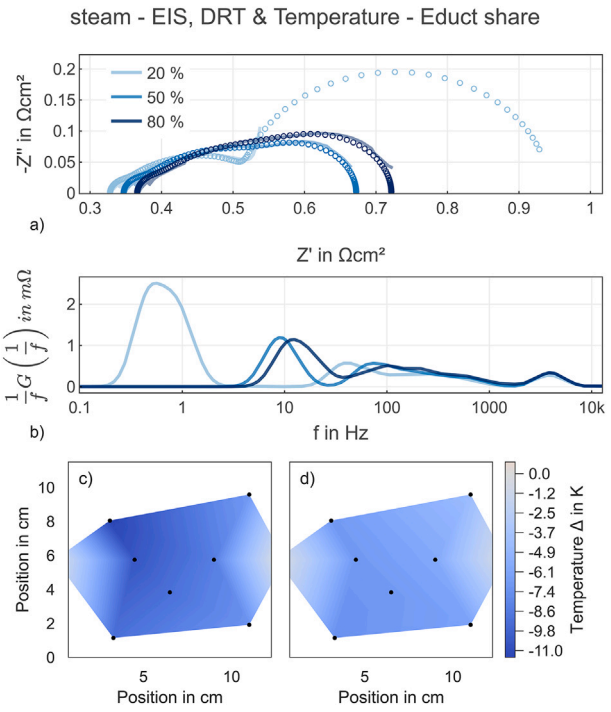

Fig. 6. (a) Nyquist and (b) DRT for educt content changes. The spatial temperature change when increasing the educt share from 20 to 50 % and from 50 to 80 % is depicted in (c) and (d), respectively. Fuel enters from the bottom and air flows from right to left in (c) and (d).

and mechanisms in the investigated stack via the Nyquist (a), DRT (b), and spatial temperature distribution plots (c) and (d).

Only subtle changes are distinguishable in the Nyquist plots, underpinning the linear nature of the effect. Increasing the current density leads to a minor increase in ohmic resistance, seen as a rightward shift of the high-frequency intercept with the x-axis in (a). The spatial temperature distribution plots (c) and (d) offer a potential explanation for this observation: increasing from 100 to 200 $\frac{mA}{cm^2}$ (subplot (c)) and from 200 to 300 $\frac{mA}{cm^2}$ (subplot (d)) results in a local temperature drop of up to 5 K in each case. This drop might have been caused by the endothermic nature of the water-splitting reaction [32]:

$$H_2O \rightarrow H_2 + \frac{1}{2}O_2; \quad \Delta H_{298\,K} = +241.7\ \text{kJ/mol} \tag{7}$$

Comparison of the DRT plots for each current density shows changes at low (~10 Hz), medium (~100–200 Hz), and high (>1000 Hz) frequencies. Low-frequency changes are associated with diffusion processes of both the fuel [8,19–25] and air electrodes [8,20,22,26] (see Fig. 3). Mid-frequency peaks are mainly correlated with air-electrode-related processes [22,23,27,29], and high-frequency processes with fuel-electrode-related processes [20,23,27,28,30]. For further details on the ongoing processes and mechanisms see Fig. 3.

Educt content

The second most influential operating parameter in steam electrolysis was the educt share, also referred to as the inlet steam fraction (H_2O_{in}). In contrast to the effect of current density, which showed only a linear behaviour, the educt content led to a non-linear change in the stack voltage. Increasing the educt share causes a non-linear decrease in the stack voltage, with a linear term of -9.70 mV $(\%_{H_2O_{in}})^{-1}$ and a quadratic term of 0.124 mV $(\%_{H_2O_{in}})^{-2}$. An explanation for this observation may be found in the Nyquist and DRT plots in Fig. 6.

While the observed increase in ohmic resistance might be attributed to a local cool-down of more than 11 K when increasing the educt share from 20 % to 50 % and from 50 % to 80 %, respectively, the non-linear nature of the voltage change appears to stem from the significant change at low frequencies, where only at low educt shares a peak of ~ 3 mΩ arises at < 1 Hz. Matching these observations with the findings from the literature review (see Fig. 3) indicates that the low-frequency peak is caused by insufficient reactant supply, which hinders diffusion to and from the reactive zones.

Table 2
Comparison of the measured voltage values for cell 2 with the sum of the calculated Nernst potential and the voltage drop from the Nyquist total resistance for steam electrolysis operation.

Educt (%)	T_{cell} (°C)	E_{Nernst} (V)	ΔE_{Nyq} (V)	E_{calc} (V)	E_{meas} (V)	ΔE (mV)
20	802	1.004	0.185	1.189	1.173	16
50	793	0.943	0.144	1.087	1.082	5
80	786	0.882	0.134	1.016	1.034	18

Note: Frequency bands in the DRT plots are indicative and may shift with the chosen regularization. The qualitative trend with educt share remains the same.

Comparing the impedance changes with the stack voltage trend in Fig. 4(a) (● line) might raise the question of why the impedance decreases from 20 % to 50 % and then increases again from 50 % to 80 %, and how this matches the monotonic decrease in stack voltage. The answer lies in the substantial change in the Nernst potential with educt share [33]:

$$E = \frac{-\Delta G_{f,H_2O}(T)}{2\,F} - \frac{RT}{2\,F}\ln\left(\frac{y_{H_2O}}{y_{H_2}\,y_{O_2}^{1/2}}\right), \tag{8}$$

where F is the Faraday constant, $\Delta G_{f,H_2O}(T)$ is the change in Gibbs free energy for water formation at temperature T, R is the universal gas constant, and y_{H_2O}, y_{H_2}, and y_{O_2} are the mole fractions at the respective electrodes. Table 2 lists the Nernst potentials E_{Nernst} corresponding to the three impedance cases in Fig. 6. These potentials are calculated using the average cell temperature T_{cell} measured by thermocouples positioned in the air-flow channels. The voltage drop derived from the impedance data, ΔE_{Nyq}, is obtained from the total resistance (low-frequency x-axis intercept) and the applied current density of 200 mA cm^{-2} (25.4 A). The calculated voltage, $E_{calc} = E_{Nernst} + \Delta E_{Nyq}$, differs from the measured voltage E_{meas} by only a few millivolts (see ΔE).

Temperature

Increasing the air-outlet temperature was found to decrease the stack voltage during steam electrolysis when all other operating parameters were held constant. The voltage decreases by 6.98 mV for a 1 K increase. In contrast to previous findings for co-electrolysis, only the isolated linear term of this effect was statistically significant in steam electrolysis [10]. This is not in conflict with earlier results, because a small dependence via current density may still exist, although within the explored range it is too small to be significant.

In Fig. 7, changes in impedance, DRT, and local temperature can be observed. Panel (a) shows a clear shift in impedance toward lower ohmic resistance as temperature increases. The corresponding DRT plot in (b) indicates changes around ~10 Hz and ~100 Hz, together with a marked reduction of the high-frequency peak (>1000 Hz). These observations follow the trend reported in the literature, where the 10 Hz-10 kHz range shows strong temperature dependence [8]. The peaks are associated with diffusion at both fuel and air electrodes for the low-frequency feature [8,19–26], gas-conversion and mass-transfer processes at mid-lower frequencies on both electrodes [19,20,22–28], and ionic or electronic transport at the fuel electrode for the high-frequency feature [20,23,27,28,30] (see Fig. 3). As shown previously, the temperature dependence of the fuel electrode and the electrolyte appears to be responsible for the observed changes [10]. DRT frequency bands

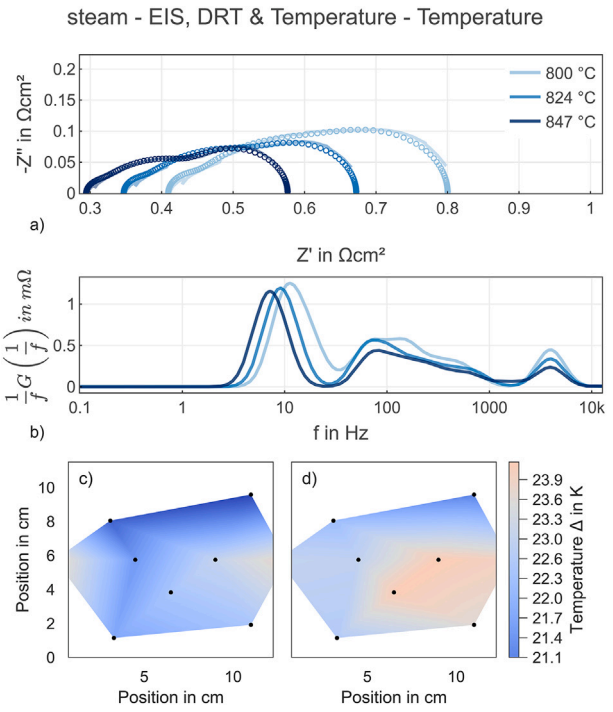

Fig. 7. (a) Nyquist and (b) DRT for air-outlet temperature changes. The spatial temperature change when increasing the air-outlet temperature from 800 to 824 °C and from 824 to 847 °C is depicted in (c) and (d), respectively. To better visualize the local change, the neutral colour between red and blue is set at $\Delta T = 23.5$ °C. Fuel enters from the bottom and air flows from right to left in (c) and (d). (For interpretation of the references to colour in this figure legend, the reader is referred to the web version of this article.)

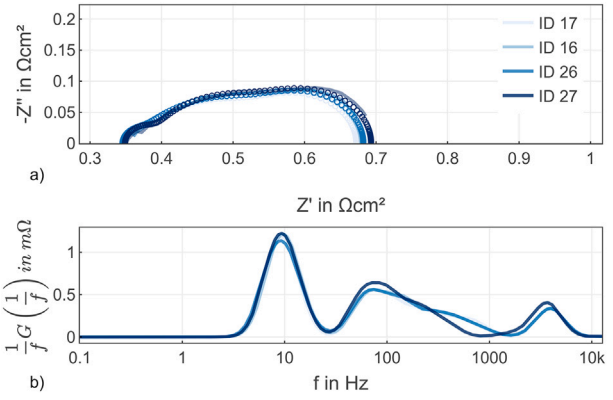

Fig. 8. Nyquist and DRT for midpoint evaluation. The same operating point was measured four times at random points in time to assess measurement variance.

are approximate and can shift with the chosen regularization, while the qualitative temperature trend remains unchanged.

3.2. Evaluation of experimental standard deviation

To quantify the variance of the measurements, the midpoint operating condition (see Table 1) was repeated four times in random order during the experimental campaign. Fig. 8 shows the Nyquist (a) and DRT (b) plots for these repetitions.

The mean total resistance was 0.682 Ω cm^2 and the standard deviation was 0.00740 Ω cm^2, which corresponds to a coefficient of variation of 1.08 %. This value is lower than the coefficient of variation of 1.86 % measured during co-electrolysis in our previous work, so we consider the repeatability sufficient for the conclusions drawn here [10]. The total resistance was taken as the low-frequency intercept on the x-axis of the Nyquist plot.

Table 3
Range of investigated operating parameters. The first four parameters were varied in both steam and co-electrolysis. The H_2x/CO_y inlet ratio was varied only in co-electrolysis.

	Low	Mid	High	Unit
Fuel flow rate	4	5.5	7	slpm
Current density	100	200	300	mA cm^{-2}
Educt content	20	50	80	%
Air-outlet temperature	800	824	847	°C
H_2x/CO_y inlet ratio	1.5	2	2.5	–

3.3. Steam vs. co-electrolysis comparison

To quantify the differences between the two modes, we compared the effect scores from the DoE evaluation in this work with those from our previous co-electrolysis study [10]. For readability the parameter ranges are summarized in Table 3. Conditions were harmonized across modes by using the identical stack and test rig, the same DoE structure and parameter ranges (current density, fuel flow, air-outlet temperature control, air flow), while feed composition necessarily differed between steam electrolysis and co-electrolysis.

The main results are:

- Within the DoE ranges, current density and air-outlet temperature have a larger impact on stack voltage in co-electrolysis than in steam electrolysis, by 10.9 % and 19.6 %, respectively.
- The influence of the educt share on voltage is smaller in co-electrolysis, and its non-linear component is reduced.
- At matched conditions and higher current densities there is a modest increase in electricity demand of about 2 % for co-electrolysis at H_2x/CO_y=2.

Fig. 9 indicates the likely mechanisms behind the stronger voltage sensitivity to current density in co-electrolysis. In panel (a) both the ohmic and total resistances are higher for co-electrolysis. In panel (b) the mid-low frequency magnitude in the range of about 20–150 Hz is larger, which is associated with diffusion, mass transfer, and toward the upper end charge-transfer processes at the fuel electrode [8,19–25]. The higher ohmic resistance aligns with the lower temperatures observed for co-electrolysis in panel (c).

According to the literature the electrolysis of CO_2 can introduce additional DRT peaks at frequencies below 10 Hz that correspond to extra losses (see the brown markers in Fig. 3). Such peaks were not detected in our data within the investigated range. This suggests that direct CO_2 electrolysis is not the dominant pathway for CO formation under our conditions. The presence of CO and CO_2 appears to hinder the electrochemical reactions slightly, especially diffusion and charge transfer as reflected in the mid-low frequency DRT range.

The effect of fuel flow rate differs by 13.3 % between modes (−19.3 versus −16.8 mV slpm^{-1}), yet its magnitude is only about 4–5 % of the current density effect. The relative change in its effect therefore needs careful interpretation, because the absolute impact is small compared with the dominant factors.

Table 4 summarizes and directly compares the effect magnitudes for both modes. These comparisons apply within the explored parameter space.

Despite these differences in per-unit effects, the resulting stack-voltage gap between modes is modest.

Fig. 10 compares matched conditions. Steam values come from this work except for the highest current density, which was measured in an additional run for this comparison. Co-electrolysis values are taken from our previous studies [10,34]. Both configurations share an air-outlet

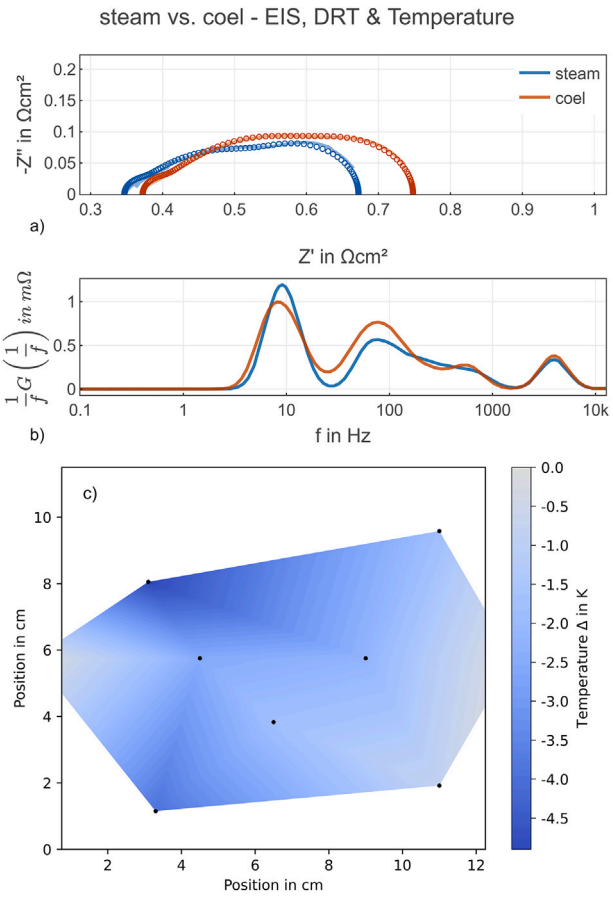

Fig. 9. (a) Nyquist and (b) DRT at the DoE midpoint for steam (blue) and co-electrolysis (orange). Panel (c) shows the temperature difference steam minus co-electrolysis. Negative values appear blue and indicate slightly lower cell temperatures in co-electrolysis. Lines in (a) indicate measurements and markers show fitted reconstructions. (For interpretation of the references to colour in this figure legend, the reader is referred to the web version of this article.)

Table 4
Comparison of effect values for operating parameters on stack voltage in steam and co-electrolysis. Co-electrolysis values are reprinted from [10]. Values rounded to three significant figures.

Effect	Steam	Co-el	Unit	Change (%)
current density	3.70	4.11	$mV \cdot (mA\,cm^{-2})^{-1}$	+10.9 %
Educt content	−9.70	−8.27	$mV \cdot (\%_{Educt})^{-1}$	−14.7 %
$T_{Air\ out}$	−6.98	−8.35	$mV \cdot K^{-1}$	+19.6 %
Educt content^2	0.124	0.083	$mV \cdot (\%_{Educt})^{-2}$	−32.9 %
Fuel flow rate	−19.3	−16.8	$mV \cdot slpm^{-1}$	−13.3 %

temperature of 824 °C, a fuel flow of 5.5 slpm, an educt share of 50 %, and current densities of 100, 200, 300, and 466.5 mA cm^{-2}. The H_2x/CO_y ratio for co-electrolysis is 2. At 200 mA cm^{-2} the error bars denote the 95 % confidence interval from the CCI midpoint repeats. The lower panel shows the relative change in stack voltages with current.

With increasing current, the voltage difference grows and co-electrolysis exhibits higher voltages. At the highest current density, the relative gap narrows to slightly above 2 %. The EIS, DRT and temperature comparison in Fig. 9 show changes below 100 Hz when switching from steam to co-electrolysis, which we attribute to diffusion-related processes based on Fig. 3. Temperature differences may also contribute, since co-electrolysis yields slightly lower stack temperatures. These observations point to a small additional loss associated with the presence of CO_2 and CO in co-electrolysis. The absence of distinct CO_2-specific DRT

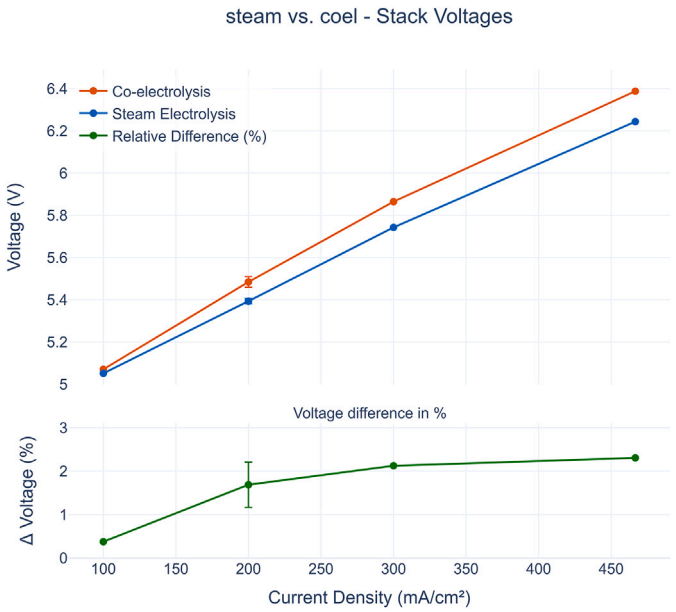

Fig. 10. Measured stack voltage for steam and co-electrolysis at 50 % educt share, 824 °C, and various current densities. Co-electrolysis is at H_2x/CO_y=2. The co-electrolysis values are from [10,34]. Error bars at 200 mA cm^{-2} show the 95 % confidence interval from the four repeated midpoint measurements. The lower panel shows the relative voltage difference of co-electrolysis versus steam.

Table 5
All investigated operational parameters in the course of the CCI test plan for steam electrolysis operation. The midpoint evaluation IDs are highlighted in bold.

ID	Current density in mA/cm^2	Temperature in °C	Fuel flow rate in slpm	Educt share	E_{Stack} in V
0	153	812	4.788	0.642	5.194
1	247	812	4.788	0.642	5.578
2	153	835	4.788	0.642	5.064
3	247	835	4.788	0.642	5.390
4	153	812	6.212	0.642	5.189
5	247	812	6.212	0.642	5.559
6	153	835	6.212	0.642	5.059
7	247	835	6.212	0.642	5.364
8	153	812	4.788	0.358	5.441
9	247	812	4.788	0.358	5.828
10	153	835	4.788	0.358	5.317
11	247	835	4.788	0.358	5.659
12	153	812	6.212	0.358	5.419
13	247	812	6.212	0.358	5.782
14	153	835	6.212	0.358	5.298
15	247	835	6.212	0.358	5.605
16	200	824	5.5	0.5	5.393
17	200	824	5.5	0.5	5.384
18	100	824	5.5	0.5	5.052
19	300	824	5.5	0.5	5.743
20	200	800	5.5	0.5	5.571
21	200	847	5.5	0.5	5.241
22	200	824	4	0.5	5.432
23	200	824	7	0.5	5.374
24	200	824	5.5	0.8	5.158
25	200	824	5.5	0.2	5.857
26	200	824	5.5	0.5	5.395
27	200	824	5.5	0.5	5.403

peaks in our previous work [10], together with the weak voltage gap at high current, may indicate that the reverse water–gas shift reaction is the dominant pathway for CO formation under the present conditions. Further work under varied conditions would be needed to confirm the contribution of RWGS across a wider space.

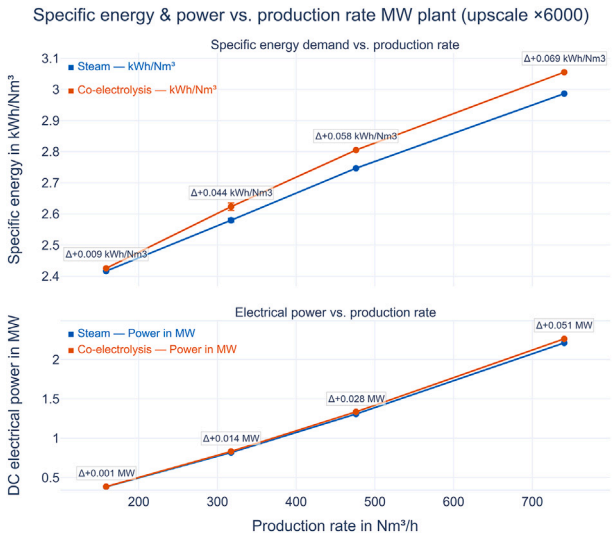

Fig. 11. Plant-scale benchmark (scaling factor ×6000) using the identical stack and test rig with matched DoE ranges. Top: specific electrical energy demand e_{Nm^3} (kWh Nm^{-3}) versus plant production (Nm^3 h^{-1}). Bottom: plant DC power (MW) versus plant production. DC stack side quantities (cell voltage, stack power, specific electricity demand) are linearly upscaled from Fig. 10 to represent a ~2.2 MW plant of 1000 stacks with 30 cells each, assuming identical cell design and operating window. Intensive metrics remain scale-invariant while power and production rate scale with active area and cell count. System-level manifold, thermal and auxiliary effects, as well as long term degradation, are not included. Error bars at 317 Nm^3 h^{-1} indicate 95 % confidence intervals from DoE midpoint experiments at 200 mA cm^{-2} (n = 4).

Fig. 10 can also be viewed as a representative IV curve for the tested electrolyte-supported stack (ESC) under the specified operating conditions. According to the stack manufacturer the recommended maximum reactant conversion on the fuel side is about 80 %. All DoE operating points were chosen such that reactant conversion remained below this limit. In addition, an extra operating point at 466.5 mA cm^{-2} was measured outside the DoE grid, which corresponds to approximately 75 % reactant conversion. This confirms that both the DoE operating window and the additional high-load point lie close to industrially relevant operation for this commercial ESC stack (Table 5).

Fig. 11 translates the observed voltage differences into a plant-scale view. At matched production rates co-electrolysis requires slightly higher DC power and specific electricity demand than steam electrolysis, consistent with the per-unit effect differences. The magnitude is small and the error bars at the centre point confirm that the difference is statistically meaningful yet practically modest within the investigated ranges. At the plant scale, the 0.051 MW higher DC power observed at 466.5 mA cm^{-2} amounts, for 7,500 h yr^{-1} operation, to ≈ 383 MWh yr^{-1} additional electricity, corresponding to about €33,000-€39,000 yr^{-1} assuming €86-€103 MWh^{-1} PPA-aligned prices. This figure refers only to DC electricity demand and electricity costs at the stack level. The additional investment and operating costs of a separate RWGS reactor and the rest of the balance of plant are not included and are outside the scope of the present study.

Note on scaling and representativeness. The experiments were conducted on a five cell stack, whereas a commercial module uses 30 cells connected in series. For the plant level comparison we apply a linear area and current scaling (factor S = 6000) to DC stack side quantities only, assuming identical cell type, geometry and materials. According to Faraday's law the molar production rate is proportional to the total current. This means it is proportional to current density multiplied by active area. In an idealised description of the stack, hydrogen and syngas production therefore scale linearly with stack area and stack current when the cell design and gas compositions are unchanged. In this representative cell description, increasing the number of identical cells in series does not change the average per cell voltage E_{cell} or the average specific electrical energy demand e_{Nm^3}. In contrast, extensive quantities such as power P and product rate $\dot{V}$ scale with active area and cell count. The tested cells share the design used in a 30 cell module, so the five cell stack is intended as a representative repeating unit of that module. A similar experimental strategy, where a single stack representative of a larger reversible SOC module is characterised on a laboratory rig and the resulting operating window is used to define operating conditions for a 150 kW rSOC module, has been reported by Königshofer et al. [9]. In practical 30 cell hotboxes, local pressure drops, gas composition gradients and temperature inhomogeneities will lead to some spread in cell performance along the stack. The invariance of intensive quantities can therefore only be expected to hold approximately. The present plant scale translation should be viewed as an illustrative application of a representative cell description. System level effects are discussed in the following paragraph and would require dedicated modelling. At full scale, several secondary effects could slightly alter the performance: manifold and header pressure losses may change local gas composition and utilisation, temperature gradients can evolve differently as module length and insulation increase, some balance-of-plant heat losses and auxiliary power demands are not represented in the stack-level model, and long-term degradation under sustained load may also influence absolute power and production values.

4. Conclusion

This work introduces a new, non-overlapping steam-electrolysis dataset on a five-cell ESC stack and provides, to our knowledge, a same-hardware benchmark against previously published co-electrolysis data under matched DoE ranges and boundary control at commercial scale. The tested cells share the design used in a 30-cell module, enabling a representative comparison.

Within steam electrolysis, the influence of inlet steam fraction, air-outlet temperature, fuel flow rate and current density on stack voltage was quantified using a central composite inscribed design and a quadratic response-surface model. EIS and DRT linked statistical effects to processes, and in-plane temperature measurements supplied spatial context. Repeatability at the midpoint condition showed a coefficient of variation of 1.08 %, indicating adequate stability for effect estimation within the explored ranges.

The main findings for steam electrolysis are:

- Current density is the primary driver of stack voltage and is approximately linear within the tested window.
- The educt share (H_2O_{in}) reduces voltage with a detectable quadratic component that is strongest at low steam fractions and weaker at higher values. Low-frequency DRT changes indicate diffusion and conversion contributions, and changes in the Nernst potential explain the overall voltage trend across the range.
- Higher air-outlet temperature lowers voltage through reductions in ohmic and charge-transfer losses, consistent with the temperature sensitivity observed in the impedance and DRT spectra.
- Fuel flow rate shows a small negative effect relative to the other factors. First-order interaction terms did not reach statistical significance at $p < 0.05$ within the present design and variance, yet modest dependencies cannot be excluded.

A same-hardware comparison with co-electrolysis under matched DoE conditions showed:

- Current density and air-outlet temperature exhibit larger per-unit effects on voltage in co-electrolysis than in steam electrolysis by 10.9 % and 19.6 % within our ranges, while the educt-share effect and its curvature are reduced.

- EIS and DRT at the midpoint indicate slightly higher ohmic and mid-to-low-frequency losses in co-electrolysis. The lower stack temperature contributes to the ohmic increase, and the mid-to-low-frequency changes are consistent with added diffusion and charge-transfer limitations in the presence of CO and CO_2. CO_2-related low-frequency DRT features reported elsewhere were not resolved under our conditions.
- At matched production rates, the plant scale translation indicates slightly higher DC power and specific electricity demand for co-electrolysis. The difference is small at about 2 % yet measurable within the reported confidence intervals. These plant scale figures are based on DC stack side scaling of a representative five cell stack and do not include system level effects such as manifold losses, auxiliary power or long-term degradation.

Taken together, these results provide a directly comparable, same-hardware benchmark and quantify where the two routes diverge within harmonized operating windows. They offer decision-ready evidence that a steam-electrolysis plus reverse water–gas shift route can achieve syngas with a slightly lower electrical demand than co-electrolysis at ($H_{2x}/CO_y = 2$) under the present conditions, while acknowledging that subtle interactions may exist outside the resolution of this study and merit further investigation.

The present analysis focuses on short-term, quasi steady-state operation and does not quantify long-term degradation behaviour. The operating sensitivities reported here are intended as a basis for designing and interpreting dedicated long-term tests. They are limited to DC stack-side quantities and do not include the cost or integration of a separate RWGS reactor or other balance-of-plant components.

5. Outlook

This study provides an overview of how key operating parameters affect stack voltage in steam electrolysis. For future work, we recommend refining and expanding the tested range, in particular toward higher current densities, so that operating windows better reflect industrial demands and allow higher hydrogen throughput.

A fair comparison of co-electrolysis with steam electrolysis plus a downstream reverse water–gas shift (RWGS) reactor requires a clearer picture of long-term stability across the key parts of the system, especially the SOE stack and the catalysts. While this work maps short-term operating sensitivities on a commercial stack, long-term stability must be assessed through dedicated tests. We suggest long runs in both modes with periodic EIS and DRT so that degradation rates can be compared directly. In parallel, the stack results should be translated into system metrics under matched product targets and heat-integration layouts, covering DC power, specific electricity demand, and a few simple cost markers. Taken together, these steps would support a robust estimate of the levelized cost of syngas for each option and help identify operating points that balance performance, durability, and plant complexity.

CRediT authorship contribution statement

Felix Mütter: Writing – original draft, Visualization, Validation, Methodology, Investigation, Formal analysis, Conceptualization. **Pavle Boškoski:** Writing – review & editing, Validation, Methodology, Data curation. **Stefan Megel:** Writing – review & editing, Resources. **Christoph Hochenauer:** Writing – review & editing, Resources, Funding acquisition. **Vanja Subotić:** Supervision, Project administration, Funding acquisition.

Declaration of competing interest

The authors declare that they have no known competing financial interests or personal relationships that could have appeared to influence the work reported in this paper.

Acknowledgement

The authors express sincere gratitude for the support received for the project “Probabilistic and explainable data-driven modeling of solid-oxide systems” jointly financed by the Slovenian Research and Innovation Agency (ARIS) (project number J2-4452) and the Austrian Science Fund (FWF), as well as for the project entitled “HyTechonomy - Hydrogen Technologies for Sustainable Economies” (Grant No. 882510) by the Austrian Research Promotion Agency (FFG). This research was funded in whole, or in part, by the Austrian Science Fund (FWF) [10.55776/I6251]. For the purpose of open access, the author has applied a CC BY public copyright licence to any Author Accepted Manuscript version arising from this submission.

Data availability

Data will be made available on request.

References

[1] European Commission. Going climate-neutral by 2050 – A strategic long-term vision for a prosperous, modern, competitive and climate-neutral EU economy. Publications Office; 2019. https://doi.org/10.2834/02074
[2] Dermühl S, Riedel U. A comparison of the most promising low-carbon hydrogen production technologies. Fuel 2023;340:127478. https://doi.org/10.1016/J.FUEL.2023.127478
[3] Zheng Y, Chen Z, Zhang J. Solid oxide electrolysis of h_2o and CO_2 to produce hydrogen and low-carbon fuels. Electrochem Energy Rev 2021;4(3):508–17. https://doi.org/10.1007/s41918-021-00097-4. https://link.springer.com/article/10.1007/s41918-021-00097-4.
[4] Peacock J, Cooper R, Waller N, Richardson G. Decarbonising aviation at scale through synthesis of sustainable e-fuel: a techno-economic assessment. Int J Hydrogen Energy 2024;50:869–90. https://doi.org/10.1016/j.ijhydene.2023.09.094
[5] Wolf SE, Vibhu V, Tröster E, Vinke IC, Eichel RA, de Haart LGJ. Steam electrolysis VS. Co-electrolysis: mechanistic studies of long-term solid oxide electrolysis cells. Energies 2022;15(15):5449. https://doi.org/10.3390/EN15155449/S1
[6] Preininger M, Subotić V, Stoeckl B, Schauperl R, Reichholf D, Megel S, Kusnezoff M, Hochenauer C. Electrochemical characterization of a CFY-stack with planar electrolyte-supported solid oxide cells in rsoc operation. Int J Hydrogen Energy 2018;43(27):12398–412. https://doi.org/10.1016/J.IJHYDENE.2018.04.230
[7] Preininger M, Stoeckl B, Subotić V, Hochenauer C. Characterization and performance study of commercially available solid oxide cell stacks for an autonomous system. Energy Convers Manag 2020;203:112215. https://doi.org/10.1016/j.enconman.2019.112215
[8] Fang Q, Blum L, Menzler NH. Performance and degradation of solid oxide electrolysis cells in stack. J Electrochem Soc 2015;162(8):F907–12. https://doi.org/10.1149/2.0941508JES/XML
[9] Königshofer B, Boškoski P, Nusev G, Koroschetz M, Hochfellner M, Schwaiger M, Juričić D, Hochenauer C, Subotić V. Performance assessment and evaluation of SOC stacks designed for application in a reversible operated 150 kw Rsoc power plant. Appl Energy 2021;283:116372. https://doi.org/10.1016/j.apenergy.2020.116372. https://www.sciencedirect.com/science/article/pii/S0306261920317487?via%3Dihub#fig3.
[10] Mütter F, Boškoski P, Megel S, Hochenauer C, Subotić V. Optimising solid oxide cells for co-electrolysis operation: parameter interactions and efficiency gains at industrial scale. Appl Energy 2025;396:126229. https://doi.org/10.1016/J.APENERGY.2025.126229
[11] Reiner D, Marković S, Schröttner H, Hochenauer C, Subotić V. Electrochemical investigation of the influence of gas compositions on industrial-sized fuel electrode supported single cells under CO- and CO_2-electrolysis conditions. J CO2 Util 2025;99:103152. https://doi.org/10.1016/J.JCOU.2025.103152. https://linkinghub.elsevier.com/retrieve/pii/S2212982025001362.
[12] Metso. HSC Chemistry 10 [software]. Pori, Finland: Metso Finland Oy; 2025. https://www.hsc-chemistry.com/.
[13] Megel S, Dosch C, Rothe S, Kusnezoff M, Trofimenko N, Sauchuk V, Michaelis A, Bienert C, Brandner M, Venskutonis A, Kraussler W, Sigl LS. CFY-stacks for use in stationary SOFC and SOEC applications. ECS Transactions 2013;57(1):89–98. https://doi.org/10.1149/05701.0089ecst. https://iopscience.iop.org/article/10.1149/05701.0089ecst/meta.
[14] Vögtlin Instruments GmbH Switzerland. Red-y smart series – thermal MASS flow meters and controllers. 2024. https://www.voegtlin.com/en/mass-flow-meters-and-controllers-for-gases/red-y-smart-series/.
[15] Megel S, Rothe S, Schöne J, Sauchuk V, Trofimenko N, Schilm J, Kusnezoff M. Degradation analysis of cfy-stacks mk35x – a guide for exact measurement. In: 14th European SOFC & SOE Forum 2020, Lucerne, Switzerland;; Dresden, Germany; 2020. https://publica-rest.fraunhofer.de/server/api/core/bitstreams/3b685700-ad1c-4b2c-8c10-6bb346561af7/content [accessed: 2025-Nov-5].
[16] Boškoski P, Debenjak A, Mileva Boshkoska B. Fast electrochemical impedance spectroscopy. Springer Briefs in Applied Sciences and Technology, no. 9783319533896, 2017. pp. 9–22. https://doi.org/10.1007/978-3-319-53390-2_2

[17] Wan TH, Saccoccio M, Chen C, Ciucci F. Influence of the discretization methods on the distribution of relaxation times deconvolution: implementing radial basis functions with drttools. Electrochim Acta 2015;184:483–99. https://doi.org/10.1016/J.ELECTACTA.2015.09.097

[18] Park KY, Lee T, Wang W, Li H, Chen F. High-performance ruddlesden–popper perovskite oxide with in situ exsolved nanoparticles for direct CO_2 electrolysis. J Mater Chem A 2023;11(39):21354–64. https://doi.org/10.1039/D3TA04122K

[19] Nechache A, Mansuy A, Petitjean M, Mougin J, Mauvy F, Boukamp BA, Cassir M, Ringuedé A. Diagnosis of a cathode-supported solid oxide electrolysis cell by electrochemical impedance spectroscopy. Electrochimica Acta 2016;210:596–605. https://doi.org/10.1016/j.electacta.2016.05.014

[20] Yan J, Chen H, Dogdibegovic E, Stevenson JW, Cheng M, Zhou XD. High-efficiency intermediate temperature solid oxide electrolyzer cells for the conversion of carbon dioxide to fuels. J Power Sources 2014;252:79–84. https://doi.org/10.1016/J.JPOWSOUR.2013.11.047

[21] Yan Y, Fang Q, Blum L, Lehnert W. Performance and degradation of an SOEC stack with different cell components. Electrochimica Acta 2017;258:1254–61. https://doi.org/10.1016/J.ELECTACTA.2017.11.180

[22] Hjalmarsson P, Sun X, Liu YL, Chen M. Durability of high performance ni–yttria stabilized Zirconia supported solid oxide electrolysis cells at high current density. J Power Sources 2014;262:316–22. https://doi.org/10.1016/J.JPOWSOUR.2014.03.133

[23] Sun X, Hendriksen PV, Mogensen MB, Chen M. Degradation in solid oxide electrolysis cells during long term testing. Fuel Cells 2019;19(6):740–47. https://doi.org/10.1002/FUCE.201900081

[24] Nuggehalli Sampathkumar S, Aubin P, Couturier K, Sun X, Sudireddy BR, Diethelm S, Pérez-Fortes M, Van herle J. Degradation study of a reversible solid oxide cell (rsoc) short stack using distribution of relaxation times (DRT) analysis. Int J Hydrogen Energy 2022;47(18):10175–93. https://doi.org/10.1016/J.IJHYDENE.2022.01.104

[25] Caliandro P, Nakajo A, Diethelm S, Van herle J. Model-assisted identification of solid oxide cell elementary processes by electrochemical impedance spectroscopy measurements. J Power Sources 2019;436:226838. https://doi.org/10.1016/J.JPOWSOUR.2019.226838

[26] Pan Z, Liu Q, Ni M, Lyu R, Li P, Chan SH. Activation and failure mechanism of la0.6sr0.4co0.2fe0.8o3-δ AIR electrode in solid oxide electrolyzer cells under high-current electrolysis. Int J Hydrogen Energy 2018;43(11):5437–50. https://doi.org/10.1016/J.IJHYDENE.2018.01.181

[27] Huang Z, Qi H, Zhao Z, Shang L, Tu B, Cheng M. Efficient CO_2 electroreduction on a solid oxide electrolysis cell with la0.6sr0.4co0.2fe0.8o3-δ-gd0.2ce0.8o2-δ infiltrated electrode. J Power Sources 2019;434:226730. https://doi.org/10.1016/J.JPOWSOUR.2019.226730

[28] Yang Y, Tong X, Hauch A, Sun X, Yang Z, Peng S, Chen M. Study of solid oxide electrolysis cells operated in potentiostatic mode: effect of operating temperature on durability. Chem Eng J 2021;417:129260. https://doi.org/10.1016/J.CEJ.2021.129260

[29] Subotić V, Futamura S, Harrington GF, Matsuda J, Natsukoshi K, Sasaki K. Towards understanding of oxygen electrode processes during solid oxide electrolysis operation to improve simultaneous fuel and oxygen generation. J Power Sources 2021;492:229600. https://doi.org/10.1016/J.JPOWSOUR.2021.229600

[30] Hjalmarsson P, Sun X, Liu YL, Chen M. Influence of the oxygen electrode and inter-diffusion barrier on the degradation of solid oxide electrolysis cells. J Power Sources 2013;223:349–57. https://doi.org/10.1016/j.jpowsour.2012.08.063

[31] International Energy Agency (IEA). Germany prices for wholesale electricity, ppas and auction ceilings, January 2021–march 2023, licence: CC BY 4.0 (2023. https://www.iea.org/data-and-statistics/charts/germany-prices-for-wholesale-electricity-ppas-and-auction-ceilings-january-2021-march-2023.

[32] Velraj S, Daramola DA, Trembly JP. A novel solid oxide electrolytic cell with reduced endothermic load for CO_2 electrolysis using (la0.80sr0.20)0.95mno3-δ cathode. J CO2 Util 2021;48:101527. https://doi.org/10.1016/J.JCOU.2021.101527

[33] Wang Y, Liu T, Lei L, Chen F. High temperature solid oxide h_2o/CO_2 CO-electrolysis for syngas production. Jun 2017. https://doi.org/10.1016/j.fuproc.2016.08.009

[34] Mütter F, Boškoski P, Megel S, Hochenauer C, Subotić V. Design of experiment investigation and model-based process parameter optimisation of industrial-sized electrolyte supported solid oxide electrolysis stack for downstream fischer–tropsch synthesis. Energy Convers Manag 2025;327:119512. https://doi.org/10.1016/j.enconman.2025.119512